ISSN 1392–1320 MATERIALS SCIENCE (MEDŽIAGOTYRA). Vol. 28, No. 3. 2022

Enhancement of the Hydrogenation and Dehydrogenation Characteristics of Mg by Adding Small Amounts of Nickel and Titanium

Myoung Youp SONG, Young Jun KWAK *

Division of Advanced Materials Engineering, Jeonbuk National University, 567 Baekje-daero Deokjin-gu Jeonju, 54896, Republic of Korea

crossref http://dx.doi.org/10.5755/j02.ms.24563

Received 04 November 2019; accepted 31 December 2019

We compared the hydrogenation and dehydrogenation properties of Mg-based alloys to which small amounts of transition elements (Ni and Ti), halides (TaF_5 and VCl_3), and complex hydrides ($LiBH_4$ and $NaAlH_4$) were added through grinding in a hydrogen atmosphere (reactive milling). Mg-1.25Ni-1.25Ti is one of the samples compared, having a composition of 97.5 wt.% Mg + 1.25 wt.% Ni and 1.25 wt.% Ti. Even though Mg-1.25Ni-1.25Ti did not have the highest initial hydrogenation rate, it had the largest quantities of hydrogen absorbed and released for 60 min and the highest initial dehydrogenation rate. In addition, Mg-1.25Ni-1.25Ti did not show the incubation period in the dehydrogenation. We thus investigated the hydrogenation and dehydrogenation properties of Mg-1.25Ni-1.25Ti in more detail. Activated Mg-1.25Ni-1.25Ti absorbed 5.91 wt.% H in 12 bar H_2 and released 5.80 wt.% H in 1.0 bar H_2 at 593 K for 60 min at n = 3. For 5 wt.% hydrogen absorption by Mg-1.25Ni-1.25Ti, 18.7 min was required at 593 K in 12 bar H_2 at n = 3. Although only small amounts of Ni and Ti were added, the hydrogenation and dehydrogenation properties of Mg were greatly improved. Ni and Ti-added Mg had a higher initial dehydrogenation rate and a larger H_d (60 min) than only Ni-added Mg, suggesting that the $TiH_{1.924}$ and NiTi formed in Mg-1.25Ni-1.25Ti play roles in the increases in the initial dehydrogenation rate and H_d (60 min), probably acting as active sites for the nucleation of the Mg-H solid solution phase.

Keywords: hydrogen absorbing materials, mechanical milling, scanning electron microscopy (SEM), X-ray diffraction, dehydrogenation temperature.

1. INTRODUCTION

As hydrogen storage methods, the followings have been developed to date [1]: storages as a gas and a liquid, storage via physical adsorption, storage as metal hydrides, storage as complex hydrides, and storage via chemical reaction. Compared to conventional high pressure gas and low temperature liquid state hydrogen storage systems, solid state hydrogen storage systems have the potential to achieve high energy efficiency, good cycle stability, high safety, and low cost. Many studies have been conducted on alloys with safety, fast performances for hydrogen release from hydrides, and high storage capacities over the last 40 years [2]. Solid state hydrogen storage systems can be applied to fuel cell, stationary hydrogen storage, submarines, heat pumps, purification/separation installation, etc. Technical system targets of US Department of Energy (DOE) for light-duty fuel cell onboard hydrogen storage system in 2020 are a system gravimetric capacity of 5.5 wt.% (1.8 kWh/kg), a system volumetric capacity of 1.3 wt.% (40 gH_2/L Sys.), operating temperature of – 40/60 °C, operational cycle life of 1500, and system fill time of 3 – 5 min [3].

Mg is a potential hydrogen storage material for use in a hydrogen energy system, as it has a high hydrogen storage capacity and is inexpensive. However, it is limited by its slow release rate of hydrogen and demanding high temperature for hydrogen release. In order to improve the reaction kinetics between hydrogen and magnesium, many studies have been carried out on alloying magnesium with a specific metal such as Ni. An Mg-Ni-H_2 system is reported favorable for hydrogen decomposition due to the formation of cracks and defects on the surface of magnesium particles and increasing their roughness [4 – 6].

Liang et al. [7] studied a nanocrystalline MgH_2-Tm system by adding Ti, V, Mn, Fe, and Ni as Tm to MgH_2 through ball milling, whereupon MgH_2 experienced drastically reduced activation energy for hydrogen release. According to this report, Ti-added MgH_2 was found to have the best hydrogen release kinetics. However, since Ti and V have strong affinity with oxygen, they concluded that the best hydrogen release kinetics was attained in Ni-added MgH_2. Unlike other transition metals, Ti did not form any hydride complexes with magnesium. Kyoi et al. [8] reported the ternary Mg-Ti-H hydride, Mg_7TiH_x, which was synthesized by mixing MgH_2 and $TiH_{1.9}$ at various molar ratios under a high temperature of 873 K and high pressure of 8 GPa. The synthesized Mg_7TiH_x had a high hydrogen release capacity and a low release temperature. Asano et al. [9] synthesized the nanostructured Mg-Ti alloy by ball milling for 200 h and observed that the Mg-Ti alloys with body-centered cubic (BCC) and face-centered cubic (FCC) structures were formed with the higher Ti content. An Mg-Ti-H phase, $MgTi_{22}H$, with a FCC structure was also reported to have been formed upon hydrogenation of $Mg_{50}Ti_{50}$ with a BCC structure [10]. It is known that when the Mg_7TiH_{16} phase is generated, the efficiency of the electrochemical hydrogen storage reaction at a high temperature is good.

* Corresponding author. Tel.: +82-10-7460-3786; fax: +82-63-270-2386
E-mail address: *twistking18@nate.com* (Y.J. Kwak)

When Ti was added to Mg-Ni or Mg_2Ni [11 – 13], Ni was added to Mg-Ti [14 – 17], or Ni and Ti were added together to Mg or MgH_2 [12, 18 – 23], and Mg, Ni, and Ti are added at the same ratio or in a relatively larger amount of each element, MgH_2, Mg_2NiH_4, and TiH_2 were formed. In view of the effects of Ni and Ti additions on the hydrogenation and dehydrogenation kinetics of Mg, researchers have studied effects of the formation of various binary and ternary hydride phases such as MgH_2, Mg_2NiH_4, and TiH_2 on the hydrogen uptake and release kinetics of Mg. Previous studies have presented a series of reports on the NiTi-related phases involved in the synthesis of Ni-Ti alloy through melting or ball milling of Ni and Ti. NiTi-related hydride phases are generated at lower temperatures than Mg hydride. Zhou and Ju [14] reported that generating hydrogen absorbing phase of Mg_2Ni and catalytic phase of NiTi played an important role for promoting the capacity of hydrogen absorption/desorption. Li et al. [24] calculated theoretically the enthalpies of formation of TiNi, MgNi, TiMg, $TiMg_3$, Ti_3Mg, and TiMg. In our previous research, reactive milling such as mechanical milling in a hydrogen atmosphere was used to improve the hydrogen release kinetics of magnesium [25 – 29]. The addition of nickel and titanium to magnesium can improve the hydrogen release kinetics of magnesium but it reduces the hydrogen capacity of magnesium.

In order not to sacrifice the hydrogen-storage capacity of the alloy too much, it would be better to add small quantities. We compared the hydrogenation and dehydrogenation properties of Mg-based alloys to which small amounts of transition elements (Ni and Ti), halides (TaF_5 and VCl_3), and complex hydrides ($LiBH_4$ and $NaAlH_4$) were added through grinding in a hydrogen atmosphere (reactive milling). Mg-1.25Ni-1.25Ti is one of the samples compared, having a composition of 97.5 wt.% Mg + 1.25 wt.% Ni and 1.25 wt.% Ti. Even though Mg-1.25Ni-1.25Ti did not have the highest initial hydrogenation rate, it had the largest quantities of hydrogen absorbed and released for 60 min and the highest initial dehydrogenation rate. In addition, Mg-1.25Ni-1.25Ti did not show the incubation period for dehydrogenation. We thus investigated the hydrogenation and dehydrogenation properties of Mg-1.25Ni-1.25Ti in more detail.

2. EXPERIMENTAL DETAILS

Samples were prepared by ball milling the following materials; pure Mg powder (particle size – 20 + 100 mesh, purity 99.8 % (metals basis), Alfa Aesar), Ni (Nickel powder, Alfa Aesar, average particle size 2.2 – 3.0 μm, 99.9 % (metals basis), C typically < 0.1 %), and Ti (~ 44 μm, purity 99.9 %, Aldrich). 1.25 wt.% Ni and 1.25 wt.% Ti were added to magnesium of 97.5 wt.% of the sample total weight. The sample was milled in a pressure of 12 bar H_2 for 6 h and at 400 rpm in a hermetically-sealed stainless-steel container (with 105 hardened steel balls, total weight = 360 g, sample to ball weight ratio = 1/45) using a planetary ball mill, (Planetary Mono Mill; Pulverisette 6, Fritsch). All sample handling was performed in a glove box under Ar atmosphere in order to prevent oxidation.

In order to track changes in the amounts of absorbed and released hydrogen with changes in time, was used a Sieverts' type hydrogenation and dehydrogenation apparatus as previously explained [29]. Half a gram of each samples was introduced in the reactor of this apparatus.

Phases in the samples after reactive milling and after hydrogenation-dehydrogenation cycling were identified by X-ray diffraction (XRD) with Cu Kα radiation, using a Rigaku D/MAX 2500 powder diffractometer. A scanning electron microscope (SEM, JSM-5900) operated at 15 kV was used to observe the microstructures of the powders.

3. RESULTS AND DISCUSSION

The quantity of the absorbed hydrogen, H_a, was defined using the sample weight as a criterion. The quantity of the released hydrogen, H_d, was also defined using the sample weight as a criterion. The quantity of hydrogen absorbed for x min is indicated as H_a (x min). The quantity of hydrogen released for x min is indicated as H_d (x min). The initial hydrogenation rate (wt.% H/min) was obtained dividing H_a (2.5 min) by 2.5 and the initial dehydrogenation rate (wt.% H/min) was obtained dividing H_d (2.5 min) by 2.5.

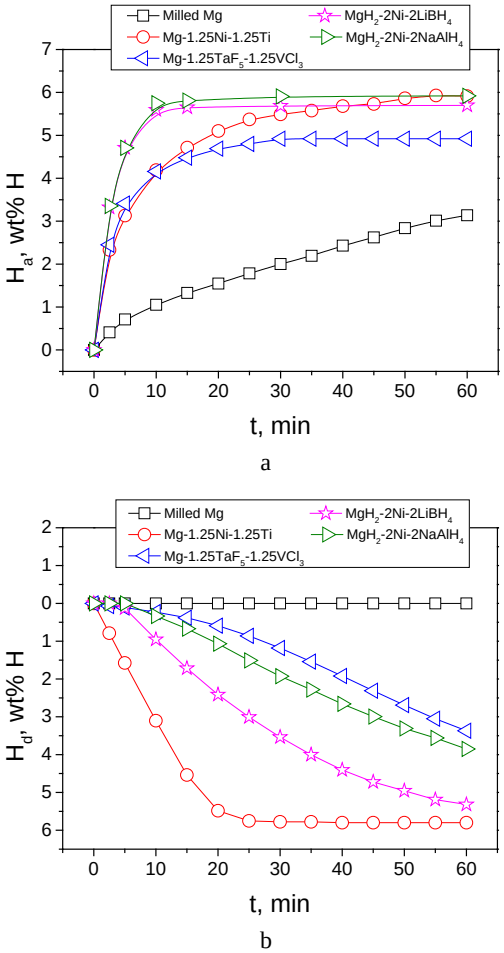

Fig. 1. a – H_a versus t curves under 12 bar H_2; b – H_d versus t curves under 1.0 bar H_2 at 593 K of the activated Mg-1.25Ni-1.25Ti, Mg-1.25TaF_5-1.25VCl_3 [30], MgH_2-2Ni-2$LiBH_4$, MgH_2-2Ni-2$NaAlH_4$, and Milled Mg [31]

We compared the hydrogenation and dehydrogenation properties of Mg-based alloys to which small amounts of transition elements, halides, and complex hydrides were added. The H_a versus time t curves in 12 bar H_2 and the H_d versus t curves in 1.0 bar H_2 at 593 K of the activated Mg-1.25Ni-1.25Ti, Mg-1.25TaF_5-1.25VCl_3 [30], MgH_2-2Ni-2$LiBH_4$, MgH_2-2Ni-2$NaAlH_4$, and milled Mg [31] are shown in Fig. 1. MgH_2-2Ni-2$NaAlH_4$ has the highest initial hydrogenation rate, followed in order by MgH_2-2Ni-2$LiBH_4$, Mg-1.25TaF_5-1.25VCl_3, Mg-1.25Ni-1.25Ti, and milled Mg. Mg-1.25Ni-1.25Ti and MgH_2-2Ni-2$NaAlH_4$ have the largest H_a (60 min), followed in order by MgH_2-2Ni-2$LiBH_4$, Mg-1.25TaF_5-1.25VCl_3, and milled Mg. The milled Mg does not release hydrogen. Mg-1.25TaF_5-1.25VCl_3, MgH_2-2Ni-2$NaAlH_4$, and MgH_2-2Ni-2$LiBH_4$ exhibit incubation periods. Mg-1.25Ni-1.25Ti shows no incubation period. After the incubation periods, Mg-1.25Ni-1.25Ti has the highest initial dehydrogenation rate, followed in order by MgH_2-2Ni-2$LiBH_4$, MgH_2-2Ni-2$NaAlH_4$, and Mg-1.25TaF_5-1.25VCl_3. Mg-1.25Ni-1.25Ti has the largest H_d (60 min), followed in order by MgH_2-2Ni-2$LiBH_4$, MgH_2-2Ni-2$NaAlH_4$, and Mg-1.25TaF_5-1.25VCl_3.

Even though Mg-1.25Ni-1.25Ti does not have the highest initial hydrogenation rate, it has the largest H_a (60 min), the highest initial dehydrogenation rate, and the largest H_d (60 min). Mg-1.25Ni-1.25Ti does not have the incubation period. We thus investigated the hydrogenation and dehydrogenation properties of Mg-1.25Ni-1.25Ti in more detail.

The XRD patterns of Mg-1.25Ni-1.25Ti and Mg after reactive milling are shown in Fig. 2. Mg after reactive milling contains Mg, a small amount of β-MgH_2, and a very small amount of γ-MgH_2. MgH_2 was formed by the reaction of Mg with hydrogen during reactive milling. Mg-1.25Ni-1.25Ti after reactive milling contains Ni and $TiH_{1.924}$ in addition to Mg, β-MgH_2, and a very small amount of γ-MgH_2. $TiH_{1.924}$ was formed by the reaction of Ti with hydrogen during reactive milling. Mg-1.25Ni-1.25Ti after reactive milling contains more MgH_2 than Mg after reactive milling, indicating that the particles of Ni and Ti-added Mg, Mg-1.25Ni-1.25Ti, are more reactive than those of Mg after reactive milling. The crystallite size of Mg in Mg-1.25Ni-1.25Ti after reactive milling (25.5 nm) was smaller than that in Mg after reactive milling (33.1 nm). The crystallite size of Mg was calculated using the Scherrer formula.

We compared the XRD pattern of Mg-1.25Ni-1.25Ti with those of the Ni and Ti-added Mg or MgH_2 samples such as Mg-14Ni-6Ti and MgH_2-10Ni-4Ti, which were dehydrogenated after hydrogenation-dehydrogenation cycling. Fig. 3 shows the XRD patterns of Ni and Ti-added Mg or MgH_2 samples, Mg-14Ni-6Ti (the number of cycles, n = 3) [22], MgH_2-10Ni-4Ti (n = 4), and Mg-1.25Ni-1.25Ti (n = 10) dehydrogenated after hydrogenation-dehydrogenation cycling. All the samples contain Mg, β-MgH_2, Mg_2Ni, Ni, $TiH_{1.924}$, NiTi, and MgO. The Mg_2Ni phase was observed which was not found in Mg-1.25Ni-1.25Ti after reactive milling. The contents of the Mg_2Ni and Ni phases increase as the content of Ni in the sample increases. The contents of the $TiH_{1.924}$, NiTi, and MgO phases increase also as the content of Ni in the sample increases. The XRD pattern of Mg-14Ni-6Ti reveals clearly the NiTi phase. In Mg-1.25Ni-1.25Ti after hydrogenation-dehydrogenation cycling, the peaks for the $TiH_{1.924}$ phase are weak.

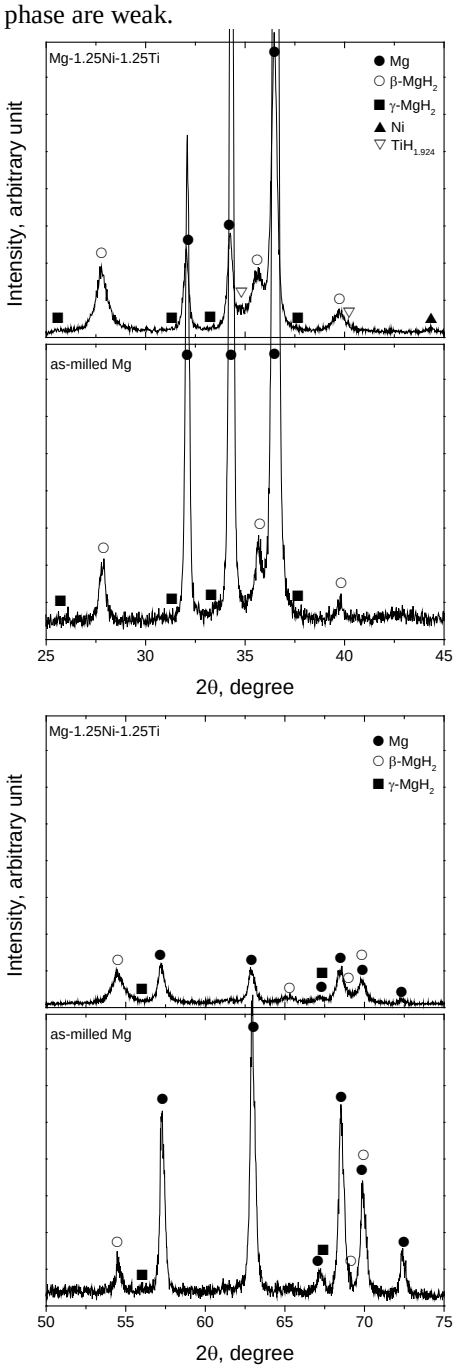

Fig. 2. XRD patterns of Mg-1.25Ni-1.25Ti and Mg after reactive milling

The crystallite size of Mg in Mg-1.25Ni-1.25Ti after hydrogenation-dehydrogenation cycling (35.8 nm) was smaller than that in Mg after hydrogenation-dehydrogenation cycling (39.3 nm).

Fig. 4 shows the SEM images of Mg-1.25Ni-1.25Ti after reactive milling and after hydrogenation-dehydrogenation cycling. The particle size of Mg-1.25Ni-1.25Ti after reactive milling is not homogeneous. The shapes of the particles are irregular. The large particles have quite flat surfaces. The particle size of Mg-1.25Ni-1.25Ti after hydrogenation-dehydrogenation cycling is not

homogeneous, either. The shapes of the particles are also irregular.

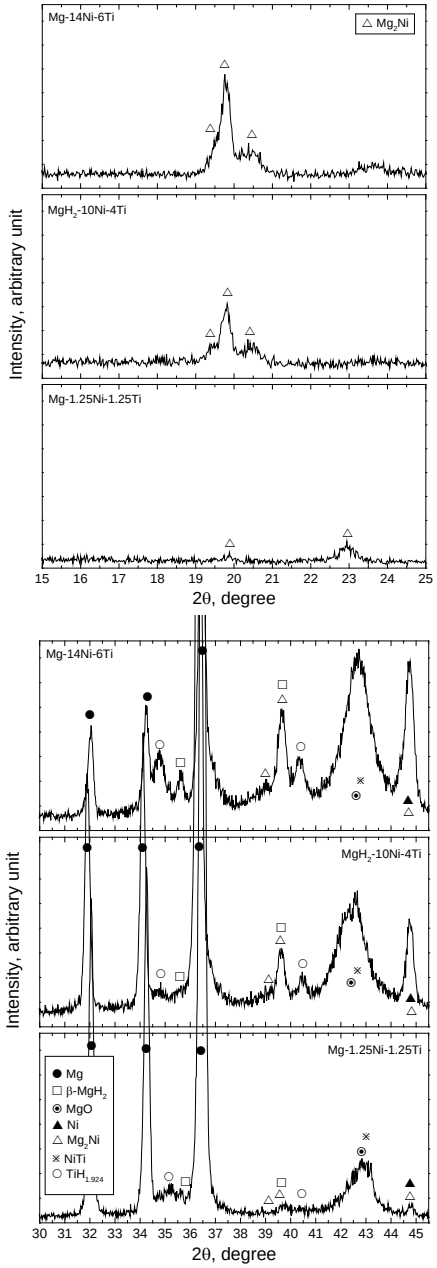

Fig. 3. XRD patterns of Mg-14Ni-6Ti (n = 3) [21], MgH_2-10Ni-4Ti (n = 4), and Mg-1.25Ni-1.25Ti (n = 10) dehydrogenated after hydrogenation-dehydrogenation cycling

The large particles are composed of fine particles. The particle sizes of Mg-1.25Ni-1.25Ti after hydrogenation-dehydrogenation cycling are slightly smaller than those of Mg-1.25Ni-1.25Ti after reactive milling. Expansion due to hydrogenation and contraction due to dehydrogenation is believed to make the particles smaller.

The sample was heated at a constant heating rate and the amount of released hydrogen was measured as a function of temperature, as described in our previous study [32]. Fig. 5 shows the desorbed hydrogen quantity H_d vs. temperature T curve and the variation, with temperature T, in the ratio of H_d change with temperature T change (dH_d/dT) together with the H_d vs. T curve for as-prepared Mg-1.25Ni-1.25Ti when the sample was heated at a heating rate of 5 ~ 6 K/min.

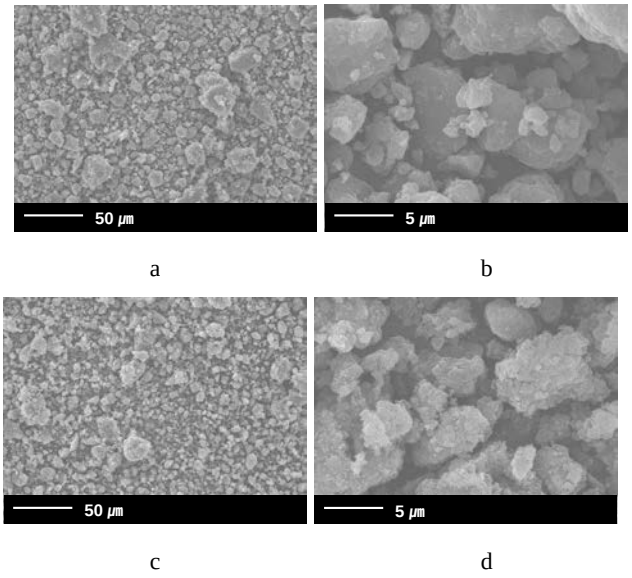

Fig. 4. SEM images of Mg-1.25Ni-1.25Ti: a, b – after reactive milling; c, d – after hydrogenation-dehydrogenation cycling

The sample begins to release hydrogen slowly at 614 K, and from 643 K it releases hydrogen very rapidly. While the sample releases hydrogen from 643 K, the temperature decreases to 633 K. The total quantity of hydrogen released is 2.23 wt.%. The decrease in temperature from 643 K to 633 K during rapid release of hydrogen is believed to be because the decrease in temperature due to endothermic release reaction is larger than the increase in temperature due to heating to increase the temperature. The sample has the largest ratio of H_d change with temperature T change (dH_d/dT) at about 633 K.

Fig. 6 shows the H_d vs. T curve after hydrogenation at n = 2, the dH_d/dT vs. T curve and H_d vs. T curve after hydrogenation at n = 2, and the H_d vs. T curves for the Mg-1.25Ni-1.25Ti samples as-milled and after hydrogenation at n = 2, when the sample was heated at a heating rate of 5 ~ 6 K/min. The sample after hydrogenation at n = 2 begins to release hydrogen rapidly at 613 K and releases rapidly to 645 K, and then from 645 K to 659 K it releases hydrogen very slowly. The total quantity of hydrogen released is 2.57 wt.%. The sample has the largest dH_d/dT at about 625 K. Comparison of the H_d vs. T curves for the samples as-milled and after hydrogenation at n = 2 shows that the temperature at which the sample begins to release hydrogen rapidly decreases from 643 K for the as-milled sample to 613 K for the sample after hydrogenation at n = 2. This indicates that after cycling the temperature for significant dehydrogenation decreases to 613 K from 643 K, the temperature for the as-milled sample. Lu et al. [20] reported that Differential Scanning Calorimetry (DSC) analysis of hydrogenated Ni/Ti-catalyzed Mg. exhibited two endothermic peaks at about 623 K (related to the dehydrogenation of Mg_2NiH_4) and 642 K (related to the dehydrogenation of MgH_2).

The variations in the H_a vs. t curve with the number of cycles, n, at 593 K in 12 bar H_2 for Mg-1.25Ni-1.25Ti are

shown in Fig. 7. At n = 1, the sample has quite a high initial hydrogenation rate and quite a large quantity of hydrogen absorbed for 60 min, H_a (60 min).

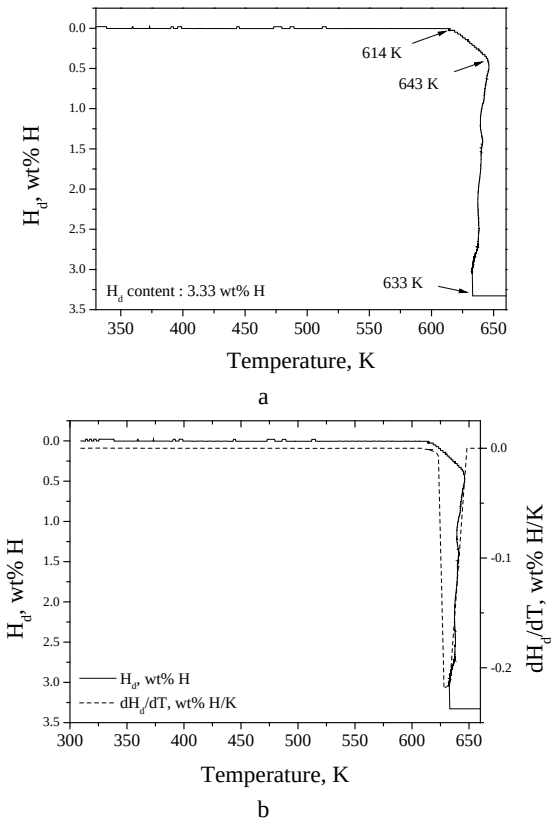

Fig. 5. a – desorbed hydrogen quantity H_d vs. temperature T curve; b – the variation, with temperature T, in the ratio of H_d change with temperature T change (dH_d/dT) together with the H_d vs. T curve for as-prepared Mg-1.25Ni-1.25Ti when the sample was heated at a heating rate of 5 ~ 6 K/min

The H_a vs. t curves show that the hydrogenation rate is quite high from the beginning to about 15 in and after about 15 min the hydrogenation rate is low. As n increases from one to eight, the initial hydrogenation rate increases and decreases from n = 8 to n = 10, in general. As n increases from one to three, the H_a (60 min) increases and decreases from n = 3 to n = 10. As n increases from three to eight, the initial hydrogenation rate increases whereas the H_a (60 min) decreases. This indicates that from n = 3 to n = 8, the particles near surface of the particles become finer while the particles inside the particles become larger due to coalescence. Table 1 shows the variations in H_a (wt.% H) as a function of t (min) at 593 K in 12 bar H_2 at n = 1, 3, 4, 7, and 10 for Mg-1.25Ni-1.25Ti. At n = 3, the sample absorbs 5.91 wt.% H.

Table 1. Variations in H_a (wt.% H) as a function of t (min) at 593 K in 12 bar H_2 at n = 1, 3, 4, 7, and 10 for Mg-1.25Ni-1.25Ti

	2.5 min	5 min	10 min	30 min	60 min
n = 1	2.02	2.83	3.52	4.6	4.83
n = 3	2.33	3.13	4.19	5.49	5.91
n = 4	2.68	3.77	4.78	5.61	5.88
n = 7	2.77	3.81	4.7	5.2	5.44
n = 10	2.58	3.53	4.19	4.55	4.69

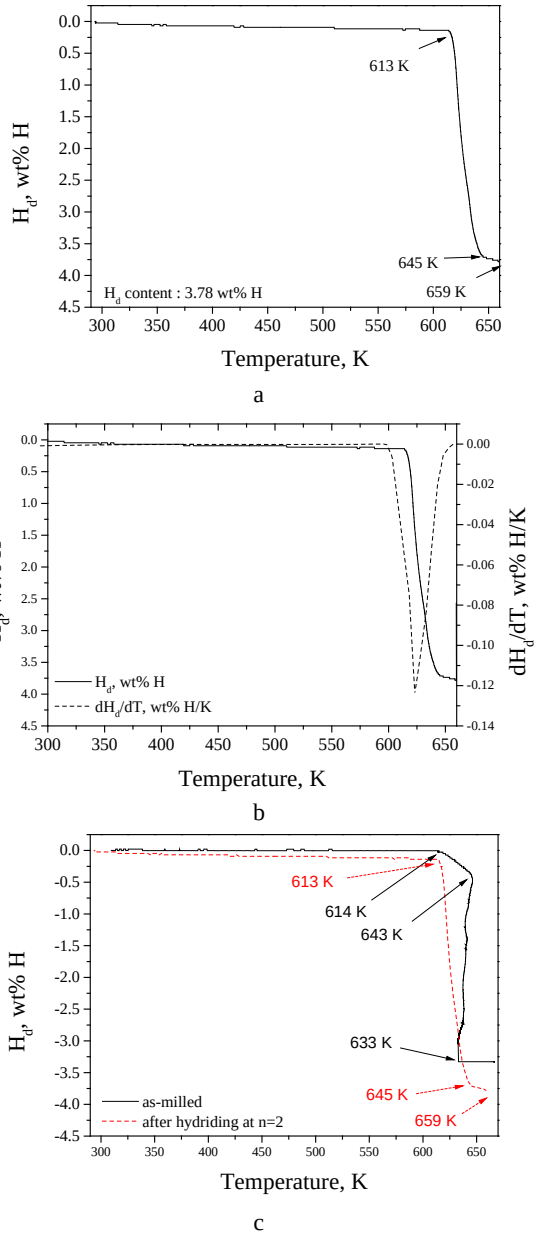

Fig. 6. a – H_d vs. T curve after hydrogenation at n = 2; b – dH_d/dT vs. T curve and H_d vs. T curve after hydrogenation at n = 2; c – H_d vs. T curves for the Mg-1.25Ni-1.25Ti samples as-milled and after hydrogenation at n = 2, when the sample was heated at a heating rate of 5 ~ 6 K/min

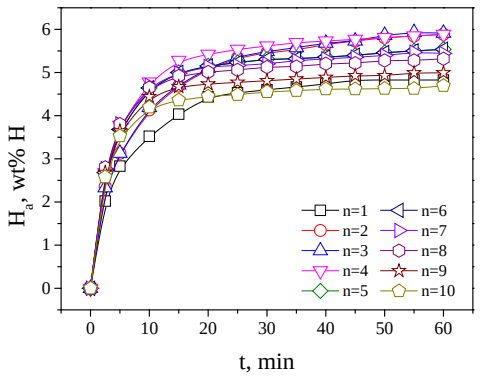

Fig. 7. Variations in the H_a vs. t curve with the number of cycles, n, at 593 K in 12 bar H_2 for Mg-1.25Ni-1.25Ti

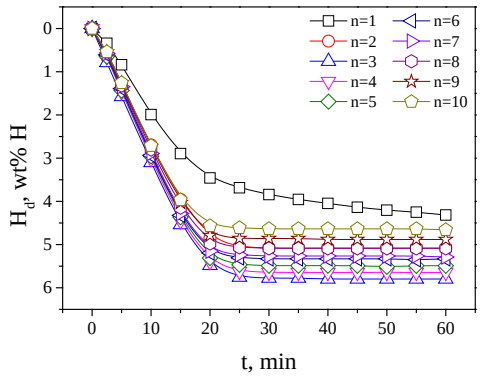

Fig. 8. Variations in the H_d vs. t curve with the number of cycles at 593 K in 1.0 bar H_2 for Mg-1.25Ni-1.25Ti

Table 2. Variations in H_d (wt.% H) as a function of t (min) at 593 K in 1.0 bar H_2 at n = 1, 3, 4, 7, and 10 for Mg-1.25Ni-1.25Ti

	2.5 min	5 min	10 min	30 min	60 min
n = 1	0.34	0.84	1.99	3.84	4.32
n = 3	0.79	1.57	3.10	5.78	5.80
n = 4	0.65	1.46	3.01	5.64	5.64
n = 7	0.58	1.34	2.89	5.26	5.29
n = 10	0.54	1.26	2.71	4.64	4.66

Fig. 8 shows the variations in the H_d vs. t curve with the number of cycles at 593 K in 1.0 bar H_2 for Mg-1.25Ni-1.25Ti. At n = 1, the initial dehydrogenation rate is quite high and the quantity of hydrogen released for 60 min, H_d (60 min), is quite large. The H_d vs. t curves show that the dehydrogenation rate is quite high from the beginning to about 20 min and after about 20 min the dehydrogenation rate is low. The initial dehydrogenation rate and H_d (60 min) increase as n increases from one to three and they decrease from n = 3 to n = 10. Table 2 shows the variations in H_d (wt.% H) as a function of t (min) at 593 K in 1.0 bar H_2 at n=1, 3, 4, 7, and 10 for Mg-1.25Ni-1.25Ti. At n = 3, the sample releases 5.80 wt.% H.

The variations in H_a (5 min) and H_a (60 min) with the number of cycles at 593 K in 12 bar H_2 for Mg and Mg-1.25Ni-1.25Ti are shown in Fig. 9.

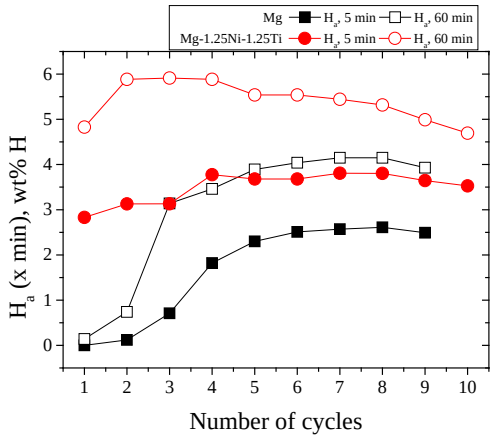

Fig. 9. Variations in H_a (5 min) and H_a (60 min) with the number of cycles at 593 K in 12 bar H_2 for Mg and Mg-1.25Ni-1.25Ti

H_a (5 min) and H_a (60 min) of Mg increase from n = 1 to n = 8 and decrease from n = 8 to n = 10. H_a (5 min) and H_a (60 min) of Mg-1.25Ni-1.25Ti increase rapidly from n = 2 to n = 5. H_a (5 min) of Mg-1.25Ni-1.25Ti increase from n = 1 to n = 4 and decrease from n = 4 to n = 10, in general. H_a (60 min) of Mg-1.25Ni-1.25Ti increase from n = 1 to n = 3 and decrease from n = 3 to n = 10. H_a (5 min) of Mg-1.25Ni-1.25Ti increase relatively rapidly from n = 1 to n = 4. H_a (60 min) of Mg-1.25Ni-1.25Ti increase relatively rapidly from n = 1 to n = 2. At each cycle, Mg-1.25Ni-1.25Ti has larger H_a (5 min) and H_a (60 min) than Mg, showing that although only small amounts of Ni and Ti were added, the hydrogenation and dehydrogenation properties of Mg are improved.

Fig. 10 shows the variations in H_d (5 min) and H_d (60 min) with the number of cycles at 593 K in 1.0 bar H_2 for Mg-1.25Ni-1.25Ti. H_d (5 min) and H_d (60 min) of Mg-1.25Ni-1.25Ti increase from n = 1 to n = 3 and decrease from n = 3 to n = 10.

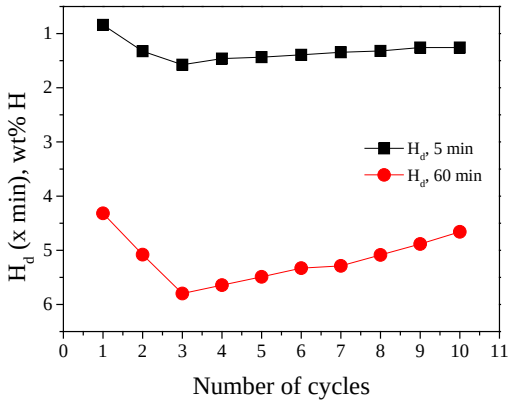

Fig. 10. Variations in H_d (5 min) and H_d (60 min) with the number of cycles at 593 K in 1.0 bar H_2 for Mg-1.25Ni-1.25Ti

Fig. 7 – Fig. 10 and Table 1, Table 2 show that the activation of Mg-1.25Ni-1.25Ti is completed after n = 3.

Reactive milling of Mg with Ni and Ti creates defects, produces clean surfaces, and decreases the particle sizes of Mg. The $TiH_{1.924}$ formed during reactive milling and its pulverization during reactive milling are believed to strengthen these effects. Hydrogenation-dehydrogenation cycling brings about similar effects due to expansion and contraction of the particles. Mg_2Ni is believed to have been formed when the sample was heated to the temperature to release the hydrogen absorbed during reactive milling [33]. The Mg_2Ni phase, with a higher dehydrogenation rate than Mg, in the sample is thought to contribute partly to the relatively high dehydrogenation rate of Mg-1.25Ni-1.25Ti. The Mg_2Ni phase has a higher dehydrogenation rate than Mg because Mg_2NiH_4 has a higher driving force for dehydrogenation (the difference between equilibrium plateau pressure and the applied hydrogen pressure) than MgH_2. The formation of the NiTi phase was also reported in the references [15, 16, 20]. The NiTi phase is believed to remain without forming its hydride because a hydrogen pressure much higher than 12 bar is required to form its hydride at 593 K.

Fig. 3 shows that Mg-1.25Ni-1.25Ti has the largest H_a (60 min), the highest initial dehydrogenation rate, and the

largest H_d (60 min), and the incubation period does not appear in the dehydrogenation of Mg-1.25Ni-1.25Ti. Fig. 3 also shows that Ni or Ni + Ti-added samples have higher initial dehydrogenation rate and larger H_d (60 min) than the milled Mg containing neither Ni nor Ti. The formed Mg_2Ni, $TiH_{1.924}$, and NiTi in Mg-1.25Ni-1.25Ti are believed to have led to these results.

It can be seen in Fig. 3 b that Ni and Ti-added Mg has a higher initial dehydrogenation rate and a larger H_d (60 min) than only Ni-added Mg. This suggests that the formed $TiH_{1.924}$ and NiTi play roles in the increases in the initial dehydrogenation rate and H_d (60 min), probably acting as active sites for the nucleation of the Mg-H solid solution phase.

Fig. 6 shows that after cycling the temperature for significant dehydrogenation decreases to 613 K from 643 K, the temperature for the as-milled sample. We believe that this phenomenon results mainly from the rapid dehydrogenation of the Mg_2NiH_4.

Table 3 shows the hydrogen storage capacities of various Mg-Ni-Ti alloys. System, composition, ball milling time, reaction temperature, reaction hydrogen pressure, and references for the various Mg-Ni-Ti alloys are given. A mark * is given for the reference in which the NiTi phase was reported. Mg-1.25Ni-1.25Ti has the largest hydrogen storage capacity among the Mg-Ni-Ti alloys. It has a hydrogen storage capacity of 5.91 wt.% at 593 K in 12 bar H_2 at n = 3. For 5 wt.% hydrogen absorption by Mg-1.25Ni-1.25Ti, 18.7 min was required at 593 K in 12 bar H_2 and for 5 wt.% hydrogen release from the hydrogenated Mg-1.25Ni-1.25Ti, 17.4 min was required at 593 K in 1.0 bar H_2, at n = 3. Mg-1.25Ni-1.25Ti was prepared by reactive milling at a revolution speed of 400 rpm for 6 h.

Zaluska et al. [35] reported that the diffusion distance of hydrogen which affects the Mg hydride growth rate can be reduced by reducing the Mg particle size via mechanical pulverization and alloying of MgH_2 together with additives. Although Liang et al. [7] added small amounts of transition metals such as Fe, Ni, and Ti to magnesium, they reduced the magnesium particle size to nanometer scale through ball milling for 20 h, lowering the hydrogen absorption reaction temperature and improving the hydrogen release amount of Mg.

4. CONCLUSIONS

We compared the hydrogenation and dehydrogenation properties of Mg-based alloys to which small amounts of transition elements (Ni and Ti), halides (TaF_5 and VCl_3), and complex hydrides ($LiBH_4$ and $NaAlH_4$) were added through grinding in a hydrogen atmosphere (reactive milling). Mg-1.25Ni-1.25Ti with a composition of 97.5 wt.% Mg + 1.25 wt.% Ni + 1.25 wt% Ti had relatively good hydrogen-storage characteristics. We thus investigated the hydrogenation and dehydrogenation properties of Mg-1.25Ni-1.25Ti in more detail. The Mg_2Ni, $TiH_{1.924}$, and NiTi formed in Mg-1.25Ni-1.25Ti are believed to have led to the results that Mg-1.25Ni-1.25Ti had the largest H_a (60 min), the highest initial dehydrogenation rate, and the largest H_d (60 min), and no incubation period in the dehydrogenation. Ni and Ti-added Mg had a higher initial dehydrogenation rate and a larger H_d (60 min) than only Ni-added Mg, suggesting that the formed $TiH_{1.924}$ and NiTi play roles in the increases in the initial dehydrogenation rate and H_d (60 min), probably acting as active sites for the nucleation of the Mg-H solid solution phase. The NiTi phase is believed to remain without forming its hydride because a hydrogen pressure much higher than 12 bar is required to form its hydride at 593 K. Mg-1.25Ni-1.25Ti has the largest hydrogen storage capacity among the Mg-Ni-Ti alloys.

Acknowledgements

This research was supported by Basic Science Research Program through the National Research Foundation of Korea (NRF) funded by the Ministry of Education (grant number NRF-2017R1D1A1B03030515).

Table 3. Hydrogen storage capacities of various Mg-Ni-Ti alloys. System, composition, ball milling time, reaction temperature, reaction hydrogen pressure, and references are given. (A mark * is given for the reference in which the NiTi phase was reported.)

System	Composition	Ball milling time, h	Reaction temperature, K	Reaction hydrogen pressure, bar	Hydrogen storage capacity, wt%	Reference
Mg-Ni-Ti	$Ti_{53}Mg_{47}Ni_{20}$	44	404	137	3.5 (SETRAM DSC 111) (DSC)	[34]
	MgH_2-Ni/Ti (4:1)	35	673	(dehydrogenation in 0.1 bar)	2.9	[18]
	$Mg_{0.5}Ti_{0.67}Ni_{0.83}$	10	RT	50	1.57	* [20]
	$Mg_{50}Ti_{16.7}Ni_{33.3}$	10	623	40	2.93	* [20]
	Mg-14Ni-6Ti	6	573	12	4.98	[22]
	Mg-1.25Ni-1.25Ti	6	593	12	5.91	* In this work
Mg_2Ni-Ti	$(Mg_2Ni)_{95}Ti_5$	15	573	0.1-101	3.88 (PCT)	[11]
MgTi-Ni	(Mg_9Ti_1)-20Ni	72	573	0.1-100	5.5 (PCT)	* [15]
	$(Mg_{0.8}Ti_{0.2})_2Ni$	6	373	12	2.5	* [16]

REFERENCES

1. **Züttel, A.** Materials for Hydrogen Storage *Mater Today* 6 (9) 2003: pp. 24 – 33. https://doi.org/10.1016/S1369-7021(03)00922-2
2. **Schlapbach, L., Züttel, A.** Hydrogen-Storage Materials for Mobile Applications *Nature* 414 2001: pp. 353 – 358. https://doi.org/10.1038/35104634
3. Technical Targets for Onboard Hydrogen Storage for Light-Duty Vehicles, *US Department of Energy*, 2016.
4. **Reilly, J.J., Wiswall, R.H.** The Reaction of Hydrogen with Alloys of Magnesium and Copper *Inorganic Chemistry* 6 (12) 1967: pp. 2220 – 2223. https://doi.org/10.1021/ic50058a020
5. **Reilly, J.J., Wiswall R.H.** The Reaction of Hydrogen with Alloys of Magnesium and Nickel and The Formation of Mg_2NiH_4 *Inorganic Chemistry* 7 (11) 1968: pp. 2254 – 2256. https://doi.org/10.1021/ic50069a016
6. **Vigeholm, B., Kjoller, J., Larsen, B., Pedersen, A.S.** Formation and Decomposition of Magnesium Hydride *Journal of the Less Common Metals* 89 (1) 1983: pp. 135 – 144. https://doi.org/10.1016/0022-5088(83)90259-X
7. **Liang, G., Huot, J., Boily, S., Van Neste, A., Schulz, R.** Catalytic Effect of Transition Metals on Hydrogen Sorption in Nanocrystalline Ball Milled MgH_2–Tm (Tm=Ti, V, Mn, Fe and Ni) Systems *Journal of Alloys and Compounds* 292 1999: pp. 247 – 252. https://doi.org/10.1016/S0925-8388(99)00442-9
8. **Kyoi, D., Sato, T., Rönnebro, E., Kitamura, N., Ueda, A., Ito, M., Katsuyama, S., Hara, S., Nore´us, D., Sakai, T.** A New Ternary Magnesium-Titanium Hydride Mg_7TiH_x with Hydrogen Desorption Properties Better than Both Binary Magnesium and Titanium Hydrides *Journal of Alloys and Compounds* 372 2004: pp. 213 – 217. https://doi.org/10.1016/j.jallcom.2003.08.098
9. **Asano, K., Enoki, H., Akiba, E.** Synthesis of HCP, FCC and BCC Structure Alloys in The Mg-Ti Binary System by Means of Ball Milling *Journal of Alloys and Compounds* 480 2009: pp. 558-563. https://doi.org/10.1016/j.jallcom.2009.01.086
10. **Asano, K., Enoki, H., Akiba, E.** Synthesis of Mg–Ti FCC Hydrides from Mg–Ti BCC Alloys *Journal of Alloys and Compounds* 478 2009: pp. 117 – 120. https://doi.org/10.1016/j.jallcom.2008.11.019
11. **Lin, C.K., Wang, C.K., Lee, P.Y., Lin, H.C., Lin, K.M.** The Effect of Ti Additions on the Hydrogen Absorption Properties of Mechanically Alloyed Mg_2Ni powders *Materials Science and Engineering* A449 2007: pp. 1102 – 1106 . https://doi.org/10.1016/j.msea.2006.02.287
12. **Li, Y.Z., Hu, F., Luo, L., Xu, J.Y., Zhao, Z.W., Zhang, Y.H.** Hydrogen Storage of Casting MgTiNi Alloys *Catalysis Today* 318 2018: pp. 103 – 106. https://doi.org/10.1016/j.cattod.2017.10.046
13. **Zheng, Q., Pivak, Y., Mooij, L.P.A., van der Erden, A.M.J., Schreuders, H., de Jongh, P.E., Bitter, J.H., Dam, B.** EXAFS Investigation of the Destabilization of the Mg–Ni–Ti (H) System *International Journal of Hydrogen Energy* 37 2012: pp. 4161 – 4169. https://doi.org/10.1016/j.ijhydene.2011.11.107
14. **Zhou, N.N., Ju, D.Y.** Study on Prsparation and Properties Evaluation of Mg/Ni/Ti Hydrogen Storage Material *International Journal of Hydrogen Energy* 39 2014: pp. 19630 – 19636. https://doi.org/10.1016/j.ijhydene.2014.09.131
15. **Hong, T.W., Kim, Y.J.** Synthesis and Hydrogenation Behavior of Mg-Ti-Ni-H Systems by Hydrogen-Induced Mechanical Alloying *Journal of Alloys and Compounds* 330 – 332 2002: pp. 584 – 589. https://doi.org/10.1016/S0925-8388(01)01507-9
16. **Borissova, A.V., Deledda, S., Hauback, B.C.** Synthesis and Hydrogen Sorption Properties of Mg-Ti-Ni Composite, Produced by Mechanical Milling at Liquid Nitrogen Temperature *Journal of Alloys and Compounds* 481 2009: pp. L24 – L26. https://doi.org/10.1016/j.jallcom.2009.03.035
17. **Anik, M.** Improvement of the Electrochemical Hydrogen Storage Performance of Mg_2Ni by the Partial Replacements of Mg by Al, Ti and Zr *Journal of Alloys and Compounds* 486 2009: pp. 109 – 114. https://doi.org/10.1016/j.jallcom.2009.06.127
18. **Lu, H.B., Poh, C.K., Zhang, L.C., Guo, Z.P., Yu, X.B., Liu, H.K.** Dehydrogenation Characteristics of Ti-and Ni/Ti-Catalyzed Mg Hydrides *Journal of Alloys and Compounds* 48 2009: pp. 152 – 155. https://doi.org/10.1016/j.jallcom.2009.02.125
19. **Ölmez, R., Çakmak, G., Öztürk, T.** Combinatorial Search for Hydrogen Storage Alloys: Mg-Ni and Mg-Ni-Ti *International Journal of Hydrogen Energy* 35 2010: pp. 11957 – 11965. https://doi.org/10.1016/j.ijhydene.2010.08.045
20. **Denys, R.V., Zavaily, I Yu., Berezovets, V.V., Paul-Boncour, V., Pecharsky, V.K.** Phase Equilibria in the Mg-Ti-Ni System at 500 °C and Hydrogenation Properties of Selected Alloys *Intermetallics* 32 2013: pp. 167 – 175. https://doi.org/10.1016/j.intermet.2012.09.010
21. **Lu, C., Zou, J.X., Shi, X.Y., Zeng, X.Q.** Synthesis and Hydrogen Storage Properties of Core-Shell Structured Binary Mg@Ti and Ternary Mg@Ti@Ni Composites *International Journal of Hydrogen Energy* 42 2017: pp. 2239 – 2247. https://doi.org/10.1016/j.ijhydene.2016.10.088
22. **Song, M.Y., Kwak, Y.J., Park, H.R., Hong, S.H.** Amelioration of The Reaction Kinetics of Mg with Hydrogen by Reactive Mechanical Grinding with Ni, Fe_2O_3, Ti or Fe *Journal of Industrial and Engineering Chemistry* 17 2011: pp. 700 – 704. https://doi.org/10.1016/j.jiec.2011.05.020
23. **Meyer, M., Mendoza-Zélis, L.** Mechanicallit Alloyed Mg-Ni-Ti and Mg-Fe-Ti Powders as Hydrogen Storage Materials *International Journal of Hydrogen Energy* 37 2012: pp. 14864 – 14869. https://doi.org/10.1016/j.ijhydene.2011.12.099
24. **Li, X.D., Elkedim, O., Nowak, M., Jurczyk, M.** Characterization and First Principle Study of Ball Milled Ti-Ni with Mg Doping as Hydrogen Storage Alloy *International Journal of Hydrogen Energy* 39 2014: pp. 9735 – 9743. https://doi.org/10.1016/j.ijhydene.2014.04.089
25. **Hong, S.H., Kwak, Y.J., Song, M.Y.** Enhancement of the Hydrogen-Storage Characteristics of Mg by Adding Mg_2Ni and Ni to MgH_2 via High Energy Ball Milling in Hydrogen Atmosphere *Korean Journal of Metals and Materials* 56 2018: pp. 59 – 65. https://doi.org/10.3365/KJMM.2018.56.1.59
26. **Hong, S.H., Song, M.Y.** Hydrogen Absorption and Release Properties of MgH_2, Mg_2Ni, and Ni-added Mg via Reactive

Mechanical Grinding *Korean Journal of Metals and Materials* 56 2018: pp. 141 – 148.
https://doi.org/10.3365/KJMM.2018.56.2.141

27. **Song, M.Y., Kwak, Y.J.** Comparison of the hydrogen release properties of $Zn(BH_4)_2$-adde d MgH_2 alloy and $Zn(BH_4)_2$ and Ni-added MgH_2 alloy *Korean Journal of Metals and Materials* 56 2018: pp. 244 – 251.
https://doi.org/DOI: 10.3365/KJMM.2018.56.3.244
28. **Song, M.Y., Choi, E., Kwak, Y.J.** Development of a Mg-Based Alloy with a Hydrogen-Storage Capacity of 7 wt% by Adding a Polymer CMC via Transformation-Involving Milling *Korean Journal of Metals and Materials* 56 2018: pp. 392 – 399.
https://doi.org/10.3365/KJMM.2018.56.5.392
29. **Song, M.Y., Baek, S.H., Bobet, J.L., Hong, S.H.** Hydrogen Storage Pproperties of a Mg-Ni-Fe Mixture Prepared via Planetary Ball Milling in a H_2 Atmosphere *International Journal of Hydrogen Energy* 35 2010: pp. 10366 – 10372.
https://doi.org/10.1016/j.ijhydene.2010.07.161
30. **Song, M.Y., Kwak, Y.J.** Hydrogen Uptake and Release Characteristics of Mg-xTaF_5-xVCl_3 (x=1.25, 2.5, and 5) *Korean Journal of Metals and Materials* 56 (8) 2018: pp. 611 – 619.
http://dx.doi.org/10.3365/KJMM.2018.56.8.611
31. **Song, M.Y., Kwak, Y.J., Lee, S.H., Park, H.R.** Comparison of Hydrogen Storage Properties of Pure Mg and Milled Pure Mg *Bulletin of Materials Science* 37 (4) 2014: pp. 831 – 835.
https://doi.org/10.1007/s12034-014-0013-6
32. **Kwak, Y.J., Park, H.R, Song, M.Y.** Changes in Microstructure, Phases, and Hydrogen Storage Characteristics of Metal Hydro-Borate and Nickel-Added Magnesium Hydride with Hydrogen Absorption and Release Reactions *International Journal of Hydrogen Energy* 42 2017: pp. 1018 – 1026.
https://doi.org/10.1016/j.ijhydene.2016.10.097
33. **Song, M.Y., Ivanov, E.I., Darriet, B., Pezat, M., Hagenmuller, P.** Hydriding Properties of a Mechanically Alloyed Mixture with a Composition Mg_2Ni *International Journal of Hydrogen Energy* 10 1985: pp. 169 – 178.
https://doi.org/10.1016/0360-3199(85)90024-2k
34. **Lomness, J.K., Hampton, M.D., Giannuzzi, L.A.** Hydrogen Uptake Characteristics of Mechanically Alloyed Mixtures of Ti-Mg-Ni *International Journal of Hydrogen Energy* 27 2002: pp. 915 – 920.
https://doi.org/10.1016/S0360-3199(01)00192-6
35. **Zaluska, A., Zaluski, L., Ström-Olsen, J.O.** Nanocrystalline Magnesium for Hydrogen Storage *Journal of Alloys and Compounds* 288 1999: pp. 217 – 225.
https://doi.org/10.1016/S0925-8388(99)0007